Materials Science-Poland, 40(3), 2022, pp. 1-11
http://www.materialsscience.pwr.wroc.pl/
DOI: 10.2478/msp-2022-0029

Deformation behaviour of high-manganese steel with addition of niobium under quasi-static tensile loading

Magdalena Barbara Jabłońska[1], Katarzyna Jasiak[2,*], Karolina Kowalczyk[2], Iwona Bednarczyk[1], Mateusz Skwarski[1], Marek Tkocz[1], Zbigniew Gronostajski[2]

[1]Silesian University of Technology, Faculty of Materials Engineering, Krasinskiego 8, 40-019 Katowice, Poland
[2]Wroclaw University of Science and Technology, Faculty of Mechanical Engineering, Lukasiewicza 5, 50-371 Wroclaw, Poland

In this paper, the heat generated during deformation under the static testing of high-manganese TWIP steel with addition of niobium was determined. The research combined the interaction of heat generated during deformation, mechanical properties, hardness and microstructure. Temperature and strain were measured simultaneously using infrared (IR) thermography and digital image correlation (DIC) method. The average temperature measured at the necked region equals 42°C at the strain rate of 0.001 s^{-1} and exceeds 100°C at 0.5 s^{-1}. Therefore at large strains, a reduction in stress was observed. The course of the hardness change coincides very well with the strain changes, however, at the strain rate of 0.5 s^{-1} near to the necking area the hardness equals to 360 HV2, whereas at the lower strain rates it equals to 370 HV2. These changes are connected mainly with increase in temperature to >100°C

Keywords: *TWIP steel, high-manganese steel, hardness, tensile testing, IR thermography, DIC*

EXPANSIONS

AHSS: advanced high-strength steel
CNC: computerized numerical control
EDM: electrical discharge machining
FLIR: a name of company specializing in thermal imaging, video analytics, etc.
GOM: a name of company specializing in measurement technology
PC: personal computer
TRIP: transformation induced plasticity steel
TWIP: twinning induced plasticity steel
UTS: ultimate tensile strength

1. Introduction

High-manganese TWIP steels exhibit a remarkable combination of high strength and ductility – this is the statement that appears ad nauseam in all papers concerning these materials. This ostensibly trivial description is, however, crucial to understand their phenomenon. The beginning of high-manganese steels can be dated to 1882, when its precursor Robert Hadfield patented the steel of 12% manganese content. Over 100 years later, Grässel and Frommeyer [1] started the first investigation of steels with the TWIP effect. In the paper published in 1998, they described the extraordinary mechanical properties of austenitic Fe–(15–30) wt.% Mn alloys, due to the effects of deformation twinning and martensitic phase transformation. At room temperature, the Fe-25Mn-3Si-3Al steel exhibited the highest elongation value of 95%, while the ultimate tensile strength reached 650 MPa.

Such remarkable results became an inspiration for other researchers to examine these materials, with a vision of their potential application in the automotive industry [2–4].

One of the most important parameters of using TWIP steels is their strain rate effect on mechanical behaviour and microstructure evolution [5, 6]. Considering that TWIP steels are promising mate-

* E-mail: katarzyna.jasiak@pwr.edu.pl

rial for manufacturing the structural components of a car body that are responsible for absorbing crash energy, it is important to recognise their dynamic deformation behaviour [7, 8].

The impact of very high strain rates on the properties and microstructure of high-Mn steel was analysed by Jabłońska et al. [9], based on the dynamic tensile tests conducted on the flywheel machine, while high strain rate compression tests performed with the split Hopkinson pressure bar confirmed the very high ability of high-manganese steels to absorb the deformation energy [10].

The above works did not take into account the analysis of the deformation temperature effect on the microstructure and mechanical properties. Nevertheless, there are many studies describing thermally activated microstructural phenomena occurring in various advanced high-strength steels. Kozłowska et al. [11] conducted static tensile tests in the temperature range from −60°C to 200°C to analyse the temperature-dependent behaviour of the metastable retained austenite in medium-Mn TRIP steel. This issue was also analysed during the wire drawing tests performed in the temperature range from 20°C to 450°C [12].

As the temperature plays a significant role in AHSS steel microstructure evolution [13], the heat generated during cold deformation must be also taken into account. Gronostajski et al. [14] performed detailed comparative analysis of this issue for DP600 and TRIP690 steels. Madivala and Bleck [15] conducted such tests for TWIP steel under quasi-static (0.01–0.5 s-1) and dynamic (1–250 s-1) conditions with the temperature measurement. For lower strain rates, the measured temperature increase at the area of fracture exceeded 100°C, while for dynamic conditions it reached 180°C. As the effect of heat generation, an increase in stacking fault energy was observed, leading to a reduction of elongation and strength of the steel subjected to dynamic tests. At dynamic condition the temperature increases even to 300°C [16].

The properties of TWIP steels are also affected by microalloying additions. Mijangos et al. [17] verified the impact of elements such as Ti, Nb, V, B and Mo. Thanks to the additions, the grain size refinement effect was obtained. The highest grain size reduction was revealed in steel with vanadium addition. Nevertheless, as the microalloying elements were in solid solution, the differences in hardness values were negligible. However, Hamada and Kömi [18] investigated the effect of microstructure on the mechanical properties for the V-microalloyed TWIP steel, proving that the ultrafine-grained microstructure contributes to a significant enhancement of these properties. Niobium addition can strongly hinder the growth of recrystallised grains; moreover, Nb atoms react with C atoms to form nanoscale NbC precipitations that can block the dislocation motion, and then the yield strength and initial work hardening ability of TWIP steel is clearly improved [19, 20].

Although undoubtedly much has already been done in the field, some aspects and phenomena concerning high-manganese TWIP steels remain unexplained or unrecognised. Hence, continuous learning about them appears to be essential in order to fully realise their potential in practical applications [21, 22].

In this paper, the heat generated during deformation under the static tensile testing of high-manganese TWIP steel with niobium addition was determined. Moreover, the attempt to evaluate its influence on the mechanical properties, hardness and microstructure was made. Temperature and strain were measured simultaneously using infrared (IR) thermography and digital image correlation (DIC) method. The novelty of this research lies not only in the combination of measurement techniques used, but also in the alloy with a unique chemical composition prepared for the study.

2. Material and experimental methods

2.1. Microstructure and chemical composition of the MnAlNb steel

The process of TWIP steel manufacturing was done at the Łukasiewicz Research Network – Institute of Ferrous Metallurgy in Gliwice, Poland. The ingots were casted in the vacuum induction furnace VSG100S from Armco iron grade 04J and pure elements of Mn, Al, C and Nb. After heat-

Table 1. Chemical composition of the examined steel [%wt]

C	Mn	Al	V	Nb	B	P	S	Ce	La	Nd	Fe
0.47	20.1	3.0	–	0.10	0.003	<0.01	0.003	0.011	0.004	0.004	rest

ing to 1,200°C, the ingots were rough-rolled in five passes with a reduction in height of about 20%–25% in every pass. Next, the obtained strips were subjected to chemical etching in order to remove the oxide layers from their surfaces, formed during the heating. The finish rolling into a thickness of ca. 3 mm was performed in five passes, after heating the strips to 1,200°C as well. Samples before tensile test were etched again and grounded. The investigations were carried out on the high-manganese MnAlNb steel belonging to the group of steels that exhibit the TWIP effect. A chemical composition of the tested steel is listed in Table 1.

The alloy was subjected to solution annealing at a temperature of 1,100°C by 2 h with water cooling. In this material state, the studied steel has the monophase austenitic microstructure with characteristic annealing twins (Figure 1).

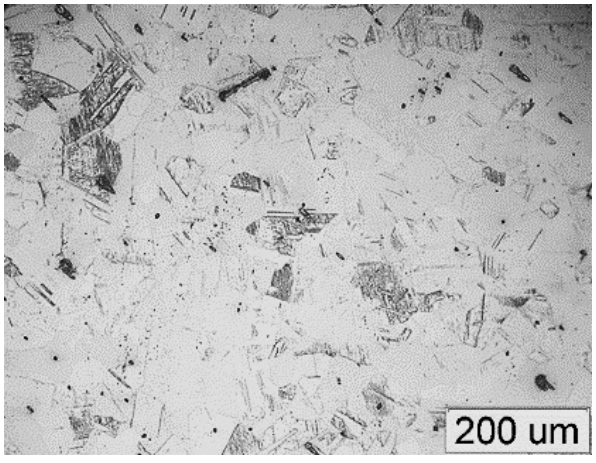

Fig. 1. Microstructure of the high-manganese MnAlNb steel after solution annealing at 1,100°C/2 h: austenite with annealing twins; the average grain diameter – 125 μm; light microscopy

2.2. Tensile tests

The tensile tests were performed at four different strain rates: 0.001 s^{-1}, 0.01 s^{-1}, 0.1 s^{-1} and 0.5 s^{-1} with the Instron 3369 universal testing machine. Variable tool velocities were applied in the tests to get the assumed, constant strain rates. For strain rates in the range of 0.001–0.1 s^{-1} specimens of gauge length of 75 mm were used (Figure 2A). Due to testing the speed limit of 500 mm min^{-1} in the Instron machine, specimens of gauge length of 14 mm (Figure 2B) had to be used to obtain the strain rate of 0.5 s^{-1}. All the specimens were cut out from the hot-rolled strip on a CNC wire cut EDM machine, with their longitudinal axes aligned with the rolling direction.

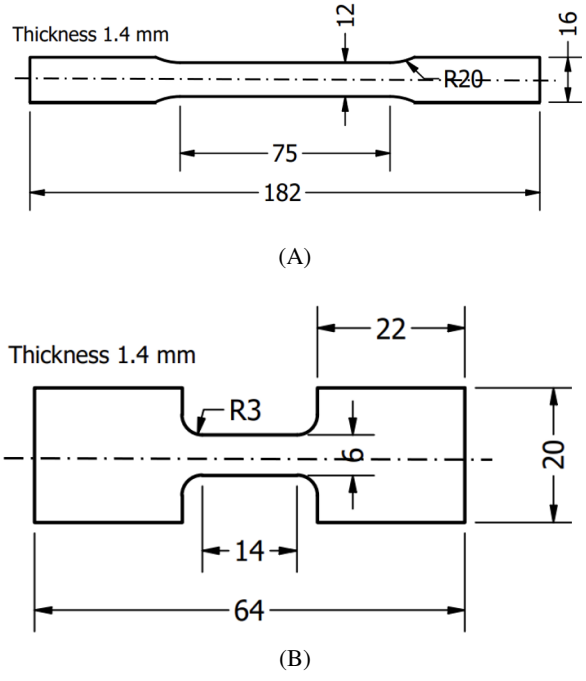

Fig. 2. Geometric features of specimens used in the tensile tests at strain rates of: **(A)** 0.001–0.1 s^{-1} and **(B)** 0.5 s^{-1}

To evaluate the effect of strain rate on the heat released in the necked region, the temperature during deformation was measured using FLIR T840 IR camera at a frame rate of 30 Hz (Figure 3A). The object temperature range was −20°C to 120°C. The accuracy of camera declared by the manufacturer equals ±2°C or ±2% of reading [23], but it

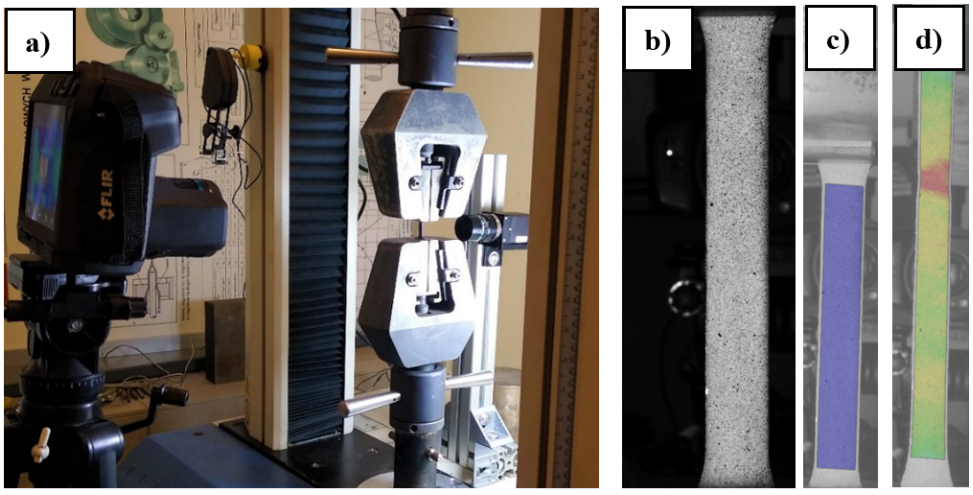

Fig. 3. The simultaneous measurement of temperature and strain during deformation: **(A)** experimental set-up for the mechanical testing, **(B)** black–white pattern for DIC measurement, **(C)** evaluation area in GOM Correlate, **(D)** example of the strain distribution image. DIC, Digital Image Correlation

can be affected by many factors. One of the most important parameters is the object emissivity – the higher it is the more accurate measurement is obtained. For this reason, the specimens were coated with black spray paint before measurement to increase their emissivity, which was then assumed to be 0.95.

Simultaneously, on the other side of the specimen, series of images were taken with the TXG50-K06 industrial camera to determine strain by the DIC method. This technique involves plotting a grid of points on the object, and then tracking and analysing the displacement of its individual points on successive images. Hence, prior to the measurements, white flexible paint was applied to the surface of the specimens as a background. Then the speckled patterns were made with black spray (Figure 3B). Analysis and determination of strain were carried out using the dedicated software GOM Correlate 2016 (Figure 3C). With the DIC technique not only was the major strain for a given evaluation area (Figure 3D) determined, but also the specimen elongation using virtual extensometer [24].

2.3. Metallographic examinations and hardness measurements

Metallographic examinations were conducted using the Olympus GX71 light microscope. Detailed observations of the microstructure were carried out using the scanning electron microscopy (SEM) technique with the Hitachi S-3400N microscope.

The observations were conducted on longitudinal sections – parallel to the specimen longitudinal axis which is aligned with the rolling direction. Sections were cut out from two selected regions (Figure 4) located closer and further from the fracture (regions A and B, respectively).

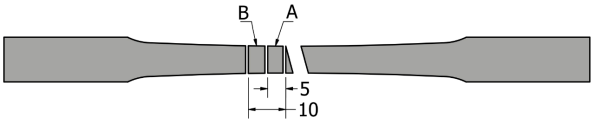

Fig. 4. Regions selected for the microstructure analysis

The hardness was measured in the selected points along the longitudinal axes of the specimens by Vickers method on the Zwick hardness tester, type 3212002/00, with a load of HV2 (20 N). The results were read with the Zwick PC-Software computer program. Moreover, hardness distribution maps were made using the results obtained from the Struers Duramin A-300D hardness tester. The input data for the hardness distribution maps were obtained from measurements made in the nodes of the measuring grid superimposed on the

Table 2. Values of UTS, total elongation and temperature of MnAlNb steel for different strain rates

Strain rate (s^{-1})	**Ultimate tensile strength, UTS (MPa)**	**Total elongation (%)**	**Average temperature in the necked region (°C)**
0.001	496	50	42
0.01	590	39	66
0.1	570	45	79
0.5	575	52	104

actual image of the tested surface. The obtained results were entered into the Surfer software, which generated a graphic image of the hardness distribution of the tested surface.

3. Results and discussion

3.1. Tensile tests results

The engineering and true stress–strain curves are presented in Figure 5, while the mechanical properties with the corresponding temperature measurement results are listed in Table 2. The total elongation value varies from 39.5% to 52.6% at 0.5 s^{-1}. The average temperature measured at the necked area equals 42°C at 0.001 s^{-1} and exceeds 100°C at 0.5 s^{-1}. The lowest yield point and tensile strength was observed at the lowest strain rate 0.001 s^{-1}. Increasing the strain rate to 0.01 s^{-1} causes an increase in the yield stress to 300 MPa and an increase in strength to 900 MPa. Further increasing the strain rate to 0.1 s^{-1} does not change the yield point. Even at the large strains, a reduction in stress was obtained, which is caused by an increase in the temperature of the sample to up to a maximum of 80°C. The strain rate increase to 0.5 s^{-1} changes the character of the stress–strain curves beginning. The large increase of the yield strength to 400 MPa is observed that is typical for the dynamic deformation; however, at large strains over 0.1, a negative strain rate sensitivity coefficient was observed at the large strains due to increase of temperature even to 100°C.

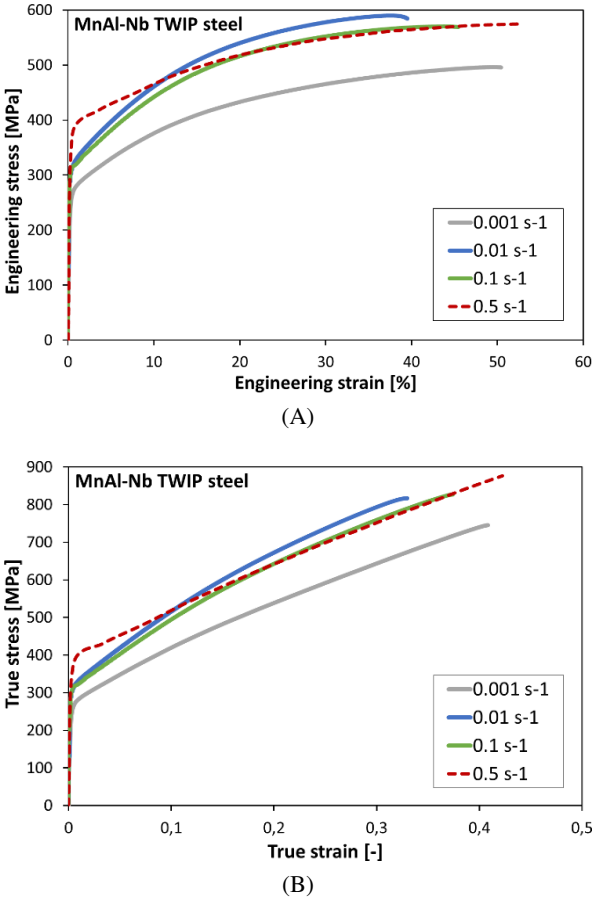

Fig. 5. The engineering **(A)** and true **(B)** stress–strain curves obtained for the MnAlNb steel from the tensile tests conducted at various strain rates

3.2. Temperature and strain distributions

The strain and temperature in a specimen during the phase of uniform elongation are obviously uniform over the gauge length. Then the strain localisation is observed, which is associated with the onset on necking. The increase in strain is accompanied by a rapid temperature increase in the necked region. The last frames with the strain and temperature distributions just before the fracture are compiled in Figure 6. For the whole range of strain rates investigated, the value of major strain exceeds 80% in the necked region and 55% in the small region close to it. Nevertheless, in the entire remaining

specimen gauge length, it equals to around 40%.

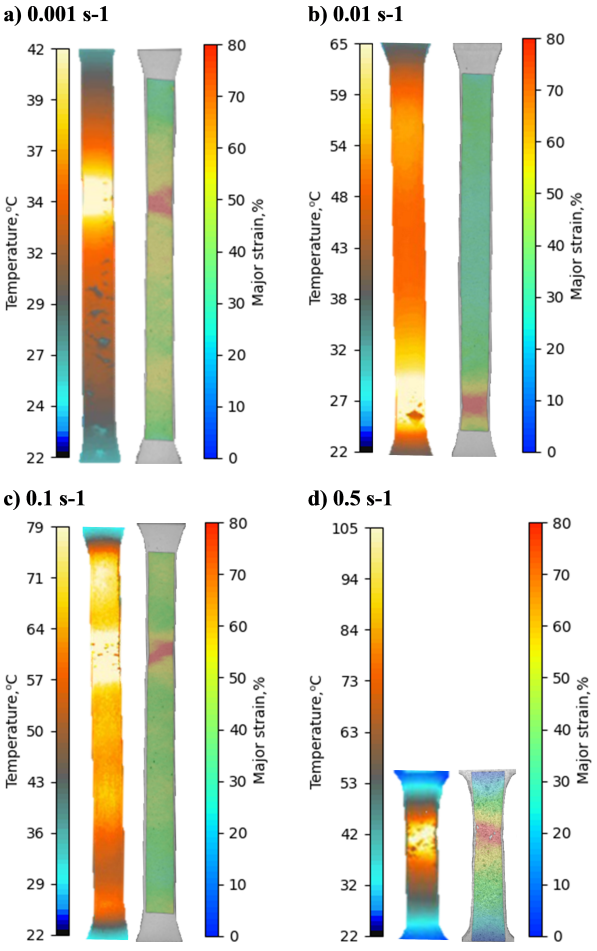

Fig. 6. Thermograms and DIC strain distribution maps at the moment just before fracture. DIC, digital image correlation

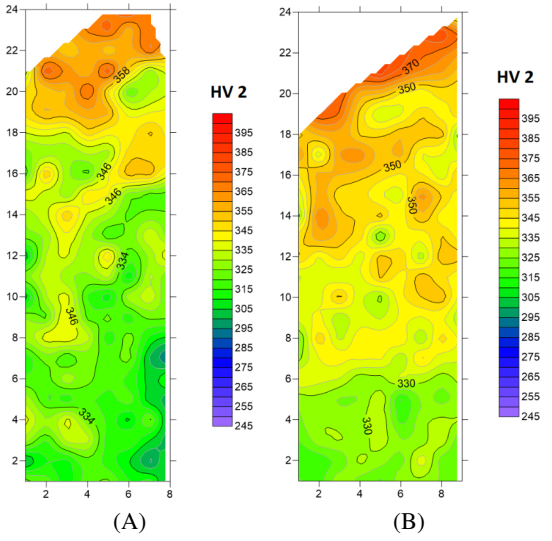

Fig. 7. The hardness distribution in one piece of the fractured specimen: **(A)** 0.001 s^{-1} and **(B)** 0.1 s^{-1}

3.3. Hardness and strain comparison

The comparison of hardness distribution in one piece of a fractured specimen after tests conducted at the strain rates of 0.001 s^{-1} and 0.1 s^{-1} is presented in Figure 7. In the specimen deformed at the strain rate of 0.001 s^{-1} the hardness rises from about 300 HV2 in the uniformly elongated region to 360 HV2 near the fracture. The increase of strain rate to 0.1 s^{-1} has caused the hardness increase in both regions: it is ca. 310 HV2 in the uniformly elongated region and exceeds 370 HV2 near the fracture.

The hardness distribution along the specimen longitudinal axis coincides very well with the major strain distribution. A comparison of these two parameters for all investigated cases is presented in Figure 8. The major strain values depending on the distance from the fracture point were extracted from the GOM Correlate Software and plotted together with the measured hardness values. The course of the hardness change coincides very well with the deformation changes; however, at the strain rate of 0.5 s^{-1} near to the necking area the hardness equals to 360 HV2, whereas at other strain rates the hardness equals to 370 HV2. These differences may be connected with increase of temperature to $>100°C$ at the highest strain rate. However, confirmation of this hypothesis requires further research. Similar observations were reported in [16]. However, for a small strain the negative values of strain rate sensitivity coefficient was also observed. In [5] is presented slightly different results, which are based on calculations, where the temperature increase for static and dynamic tests is similar, which is not obvious compared with other works.

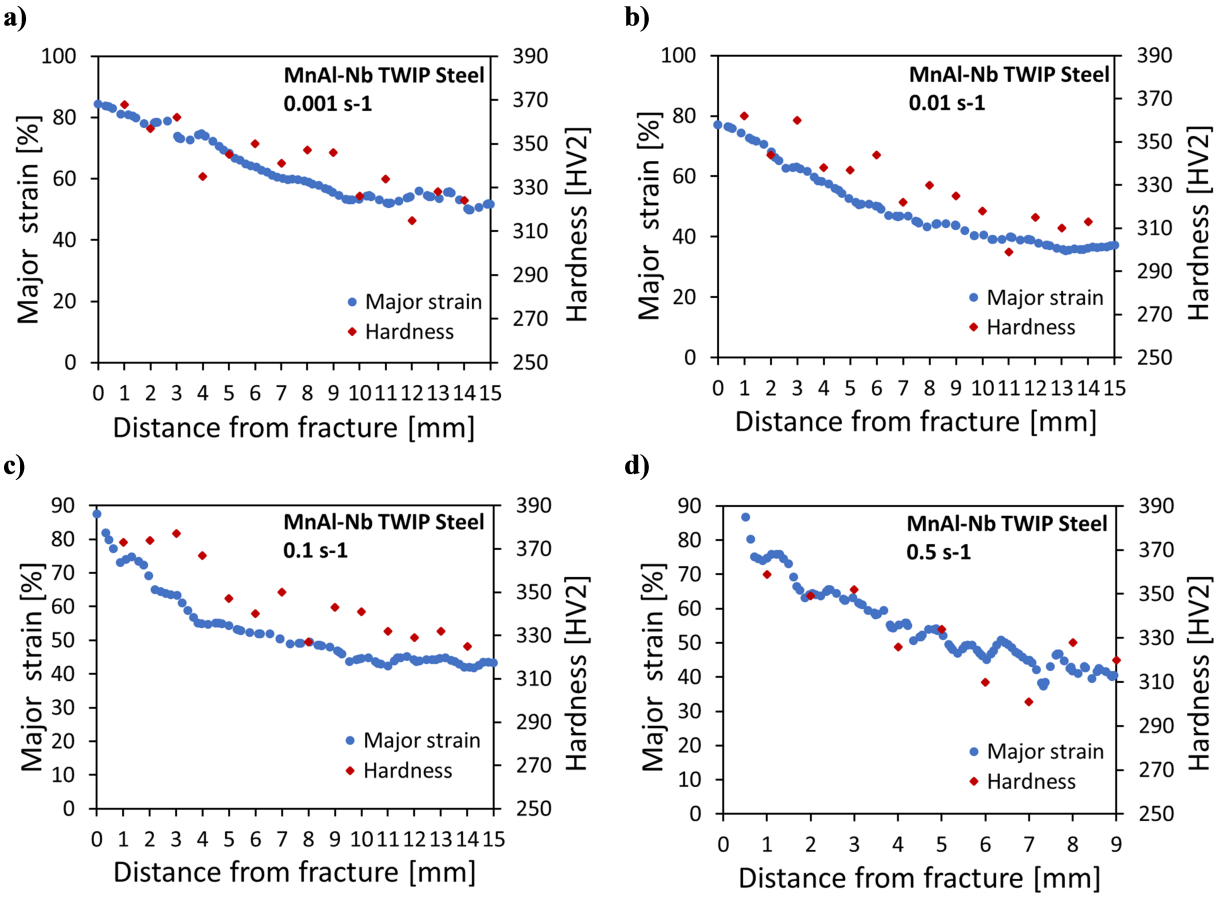

Fig. 8. Dependence of the major strain and hardness value on a distance from the fracture: a) 0.001 s^{-1}, b) 0.01 s^{-1}, c) 0.1 s^{-1}, d) 0.5 s^{-1}

3.4. Microstructure analysis

In every specimen subjected to the tensile tests conducted at the whole range of strain rates investigated, the austenite grains elongated in the tensile force direction, and both the mechanical twins and deformation bands can be observed in the microstructure of the tested steel (Figures 9 and 10). The share of twins as well as deformation bands in the microstructure rises with the increase in strain rate. SEM analysis revealed that the twinning process is dominant in the selected regions near the fracture. Both the single deformation twins and intersecting bundles of deformation twins have been identified. This is especially visible at the specimen deformed at the largest strain rate (0.5 s^{-1}), which leads to the conclusion that the increase in strain rate intensifies the activation of several slip and twinning systems as well as mutual intersection of the deformation twins (Figure 10). Observations of the microstructure were carried out in two regions: A – located closer and B – located further from the fracture. Region A corresponds to a necking and in this area, according to Figure 6, the strain amounts to even 70%, while in region B there is a much smaller strain of about 50%. This is confirmed by observations of the microstructure. In region A the grains are much more elongated in the horizontal direction than in region B. The difference between these two regions for the sample deformed at a strain rate of 0.5 s^{-1} is not so visible because the sample length was smaller.

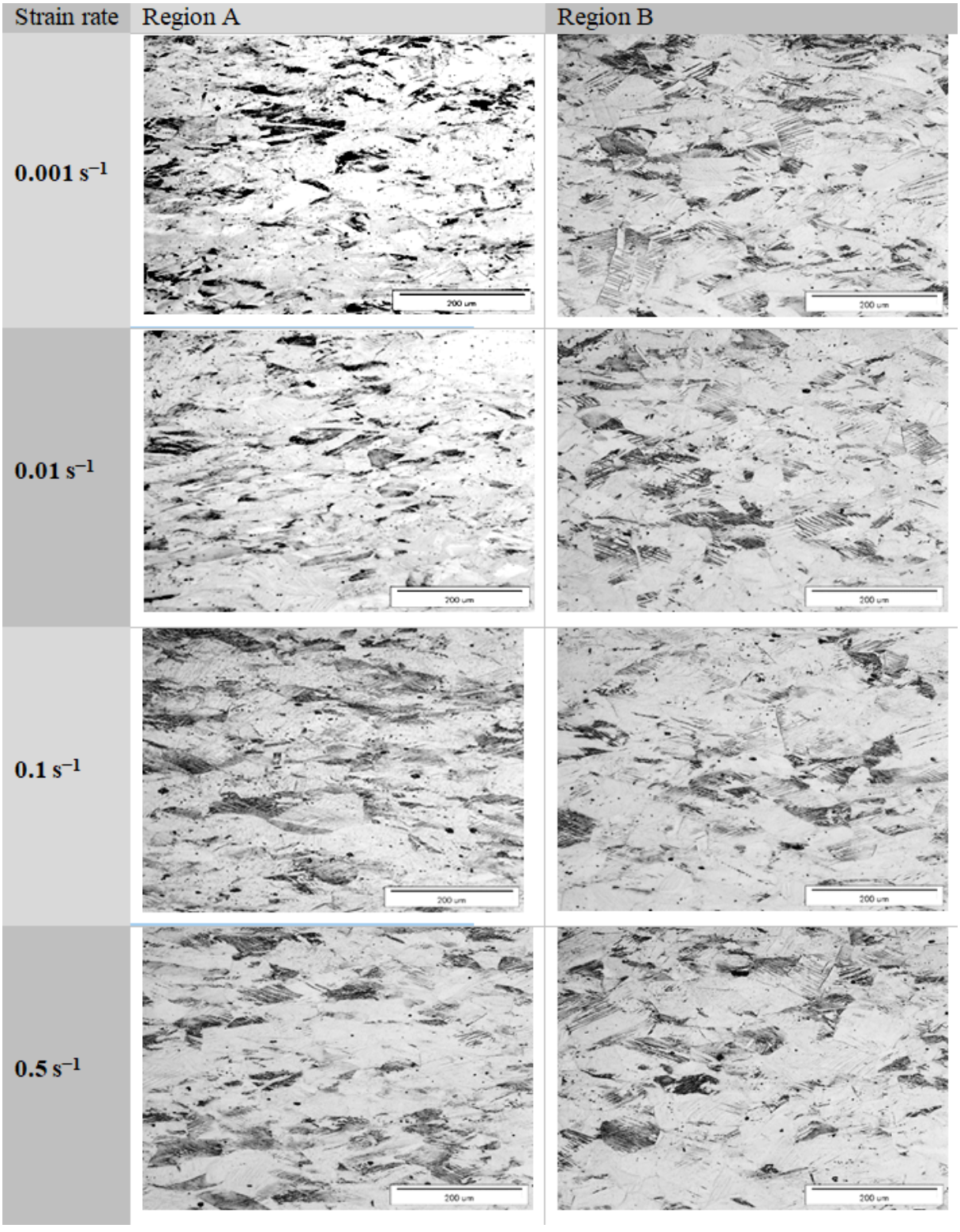

Fig. 9. Microstructure of MnAl-Nb steel deformed at various strain rates; longitudinal sections taken in regions A and regions B; light microscopy

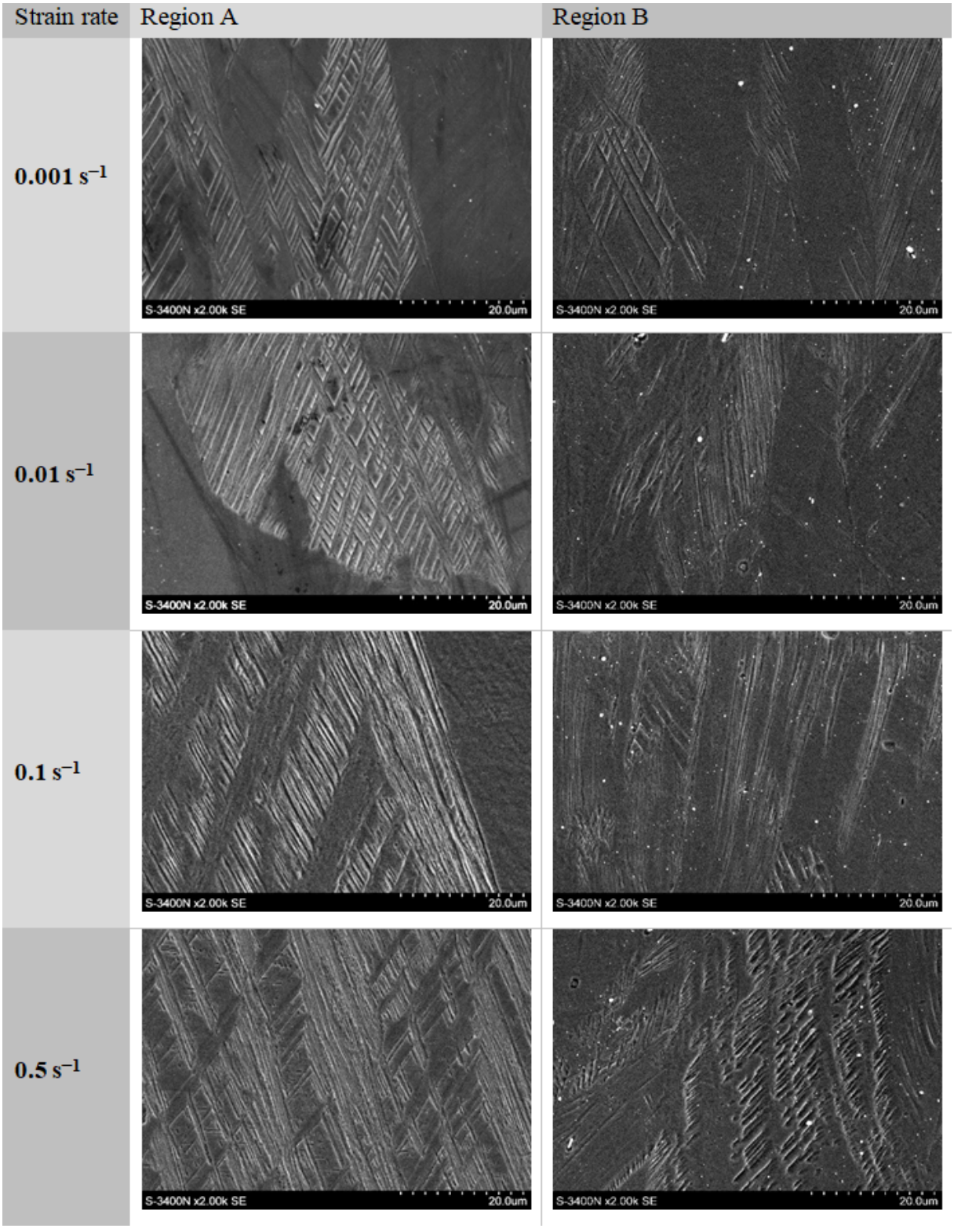

Fig. 10. Microstructure of MnAlNb steel deformed at various strain rates in the regions A and B, SEM. SEM, scanning electron microscopy

4. Conclusions and remarks

- A relatively high level of flow stress which is characteristic for the analysed TWIP steel causes generation of a large amount of heat during static and quasi-static tensile tests, due to dissipation of the deformation work. The average temperature measured at the necked area equals 42°C at the strain rate of 0.001 s^{-1} and exceeds 100°C at 0.5 s^{-1}. Therefore, at the higher strain rates, a reduction in flow stress was observed.
- The strain rate increasing to 0.5 s^{-1} changes the character of the stress–strain curves beginning. The large increase in the yield point to 400 MPa is observed that is typical for the dynamic deformation; however, for the large strains over 0.1 the negative strain rate sensitivity coefficient was observed due to the increase in temperature even to 100°C.
- The course of the hardness change coincides very well with the deformation changes; however, at the strain rate of 0.5 s^{-1} near to the necking area the hardness equals to 360 HV2, whereas for other strain rates the hardness equals to 370 HV2. These changes are connected mainly with the increase in temperature above 100°C.
- In the analysed MnAl steel with the 0.1% Nb addition the strain-induced twinning effect is still the main plastic deformation mechanism in a whole investigated range of deformation parameters. The activation of several slip and twinning systems as well as mutual intersection of the deformation twins was observed for all strain rates. Nb microaddition affects the initial grain size during solution annealing by inhibiting the austenite grain growth.

Acknowledgements

Work carried out within the framework of the project UMO-2019/35/B/ST8/02184 'Effect of the heat generated during deformation at high strain rates on the structure and properties of high manganese steels with twinning as the dominant deformation mechanism' was financed by The NCN.

References

[1] Grässel O, Frommeyer G. Effect of martensitic phase transformation and deformation twinning on mechanical properties of Fe-Mn-Si-Al steels. Mater Sci Technol. 1998;14(12):1213–7; https://doi.org/10.1179/mst.1998.14.12.1213

[2] Yuan GW, Huang MX. Supper strong nanostructured TWIP steels for automotive applications. Prog Nat Sci Mat Int. 2014;24(1):50–5; https://doi.org/10.1016/j.pnsc.2014.01.004

[3] Palma-Elvira ED, Garnica-Gonzalez P, Pacheco-Cedeño JS, Cruz Rivera JJ, Ramos-Azpeitia M, Garay-Reyes CG, et al. Microstructural development and mechanical properties during hot rolling and annealing of an automotive steel combining TRIP/TWIP effects. J Alloys Compd. 2019;798:45–52; https://doi.org/10.1016/j.jallcom.2019.05.130

[4] Kozłowska A, Grajcar A, Janik A, Radwański K, Krupp U, Matus K, et al. Mechanical and thermal stability of retained austenite in plastically deformed bainite-based TRIP-aided medium-Mn steels. Arch Civ Mech Eng. 2021;21:3; https://doi.org/10.1007/s43452-021-00284-6

[5] Wang C, Cai W, Sun C, Li X, Qian L, Jiang J. Strain rate effects on mechanical behavior and microstructure evolution with the sequential strains of TWIP steel. Mater Sci Eng A. 2022;835:142673; https://doi.org/10.1016/j.msea.2022.142673

[6] Grajcar A, Borek W. Thermo-mechanical processing of high-manganese austenitic TWIP-type steels. Arch Civ Mech Eng. 2008;8:29–38; https://doi.org/10.1016/S1644-9665(12)60119-8

[7] Cai W, Wang C, Sun C, Qian L, Fu MW. Microstructure evolution and fracture behaviour of TWIP steel under dynamic loading. Mater Sci Eng. 2022;851:143657; https://doi.org/10.1016/j.msea.2022.143657

[8] Barati Rizi MH, Ghiasabadi Farahani M, Aghaahmadi M, Kim JH, Karjalainen LP, Sahu P. Analysis of strain hardening behavior of a high-Mn TWIP steel using electron microscopy and cyclic stress relaxation. Acta Mater. 2022;240:118309; https://doi.org/10.1016/j.actamat.2022.118309

[9] Jabłońska MB, Śmiglewicz A, Niewielski G. The effect of strain rate on the mechanical properties and microstructure of the high-Mn steel after dynamic deformation tests. Arch Metall Mater. 2015;60(2A):577–80; https://doi.org/10.1515/amm-2015-0176

[10] Jabłońska MB, Kowalczyk K. Microstructural aspects of energy absorption of high manganese steels. Procedia Manuf. 2019;27:91–7; https://doi.org/10.1016/j.promfg.2018.12.049

[11] Kozłowska A, Radwański K, Matus K, Samek L, Grajcar A. Mechanical stability of retained austenite in aluminum-containing medium-Mn steel deformed at different temperatures. Arch Civ Mech Eng. 2021;21(1): 324-38; https://doi.org/10.1007/s43452-021-00177-8

[12] Wiewiórowska S, Muskalski Z, Siemiński M. The analysis of "hot" drawing process of trip steel wires at different initial temperatures. Arch Metall Mater. 2016;61(4):1991–4; https://doi.org/10.1515/amm-2016-0321

[13] Pierce DT, Benzing JT, Jiménez JA, Hickel T, Bleskov I, Keum J, et al. The influence of temperature on the strain-hardening behavior of Fe-22/25/28Mn-3Al-3Si TRIP/TWIP steels. Materialia. 2022;22:101425; https://doi.org/10.1016/j.mtla.2022.101425

[14] Gronostajski Z, Niechajowicz A, Kuziak R, Krawczyk J, Polak S. The effect of the strain rate on the stress-strain curve and microstructure of AHSS. J Mater Process Technol. 2017;242:246–59; https://doi.org/10.1016/j.jmatprotec.2016.11.023

[15] Madivala M, Bleck W. Strain rate dependent mechanical properties of TWIP steel. JOM. 2019;71(4):1291–302; https://doi.org/10.1007/s11837-018-3137-0

[16] Soares GC, Vázquez-Fernández NI, Hokka M. Thermo-mechanical behavior of steels in tension studied with synchronized full-field deformation and temperature measurements. Exp Tech. 2021;45(5):627–43; https://doi.org/10.1007/s40799-020-00436-y

[17] Mijangos D, Mejia I, Cabrera JM. Influence of microalloying additions (Nb, Ti, Ti/B, V and Mo) on the microstructure of TWIP steels. Metall Microstruct Anal. 2022;11(3):524–36; https://doi.org/10.1007/s13632-022-00871-w

[18] Hamada A, Kömi J. Effect of microstructure on mechanical properties of a novel high-Mn TWIP stainless steel bearing vanadium. Mater Sci Eng A. 2018;718:301–4; https://doi.org/10.1016/j.msea.2018.01.132

[19] Bai Y, Jiao D, Li J, Yang Z. Effect of Nb content on the stacking fault energy, microstructure and mechanical properties of Fe-25Mn-9Al-8Ni-1C alloy. Mater Today Commun. 2022;31:103554; https://doi.org/10.1016/j.mtcomm.2022.103554

[20] Li D, Feng Y, Song S, Liu Q, Bai Q, Wu G, et al. Influences of Nb-microalloying on microstructure and mechanical properties of Fe-25Mn-3Si-3Al TWIP steel. Mater Des. 2015;84:238–44; https://doi.org/10.1016/j.matdes.2015.06.092

[21] Chandan AK, Tripathy S, Sen B, Ghosh M, Ghosh Chowdhury S. Temperature dependent deformation behavior and stacking fault energy of Fe40Mn40Co10Cr10 alloy. Scr Mater. 2021;199:113891; https://doi.org/10.1016/j.scriptamat.2021.113891

[22] Lee JY, Hong JS, Kang SH, Lee YK. The effect of austenite grain size on deformation of Fe–17Mn steel. Mater Sci Eng A. 2021;809:140972; https://doi.org/10.1016/j.msea.2021.140972

[23] FLIR. FLIR T840^{TM} QUICKLY MAKE CRITICAL DECISIONS. 2019. [Online]. Available: https://www.testequipmentdepot.com/flir/pdf/t840_datasheet.pdf. Accessed 14 Nov 2022.

[24] Wang YH, Jiang JH, Wanintrudal C, Zhou D, Smith LM, Yang LX. Whole field sheet-metal tensile test using digital image correlation. Exp Tech. 2010;34(2):54–9; https://doi.org/10.1111/j.1747-1567.2009.00483.x

Received 2022-10-29
Accepted 2022-11-17